A comparison of 18F-FDG PET/MR with PET/CT in pulmonary tuberculosis

Benjamin A. Thomas[1,2], James S. Molton[3,4], Francesca Leek[1], Yan Pang[4], John J. Totman[1], Nicholas I. Paton[3,4], David W. Townsend[1]

[1]Agency for Science Technology and Research - National University of Singapore Clinical Imaging Research Centre, Singapore

[2] Institute of Nuclear Medicine, University College London, London, United Kingdom

[3] Yong Loo Lin School of Medicine, National University of Singapore, Singapore

[4] University Medicine Cluster, National University Health System, Singapore

Corresponding author:

Benjamin A. Thomas, PhD
Institute of Nuclear Medicine
University College London Hospital (T-5)
235 Euston Road
London NW1 2BU
United Kingdom

E-Mail: b.a.thomas@ucl.ac.uk
ORCID: 0000-0002-9784-1177

Running title: TB PET/MR and PET/CT comparison

Keywords: pulmonary tuberculosis, PET/CT, PET/MR, multi-modal imaging

Word count: 4424

ABSTRACT

Purpose: PET/CT has been shown to detect lesions in patients with pulmonary tuberculosis (PTB) and may be of value for assessing PTB disease in clinical research studies. However, radiation dose is of concern for clinical research in individuals with an underlying curable disease. This study aimed to determine whether PET/MR is equivalent to PET/CT in PTB.

Methods: Ten patients with microbiologically-confirmed PTB were recruited. Patients received 129.0 ± 4.1 MBq of 18F-FDG. Five of the ten patients underwent a PET/MR scan, followed by PET/CT. The remaining five were first imaged on the PET/CT followed by the PET/MR imaging. PET acquisition began at 66.7 ± 14.4 minutes (mean ± standard deviation [s.d.]) post-injection (p.i.) when performing PET/MR first (PET/CT: 117.2 ± 5.6 minutes), and 92.4 ± 7.6 minutes when patients were imaged on PET/MR second (PET/CT: 61.1 ± 3.9 minutes). PET data were iteratively reconstructed with Ordinary-Poisson Ordered-Subset Expectation-Maximisation (OP-OSEM) and reconstruction parameters were matched across the two scanners. A visual lesion detection task and SUV analysis was performed. The CT Hounsfield unit values of PTB lesions were also compared to MR-based attenuation correction (MRAC) mu-map tissue classes.

Results: 108 PTB lesions were detected on PET/MR and 112 on PET/CT. SUV analysis was performed on 50 of these lesions that were observed with both modalities. SUVmean and SUVmax were significantly lower on PET/MR (SUVmean: 2.6 ± 1.4; SUVmax: 4.3 ± 2.5) than PET/CT (SUVmean: 3.5 ± 1.5; SUVmax: 5.3 ± 2.4).

Conclusions: PET/MR visual performance was shown to be comparable to PET/CT in terms of the number of PTB lesions detected. SUVs were significantly lower on PET/MR. Dixon-based attenuation correction under-estimates the linear attenuation coefficient of PTB lesions, resulting in lower SUVs compared to PET/CT. However, use of PET/MR to measure the response of lung lesions to assess response to treatment in research studies is unlikely to be affected by these differences in quantification.

INTRODUCTION

Several recent studies have indicated that PET/CT has an important role to play in tuberculosis research, in particular for the detection of subclinical tuberculosis [1-6]. Soussan et al. identified two distinct patterns when imaging PTB using PET/CT: the *lung pattern* and *lymphatic pattern* [7]. The former describes a pattern of restricted and mildly hypermetabolic infection, while the latter is observed as an intense and systemic infection. However, in patients with a curable disease, such as TB, the radiation dose associated with PET/CT is a significant limitation for research studies that require longitudinal assessment of outcomes with serial scans. In this respect the newer technology of PET/MRI may have a distinct advantage.

Although many studies have compared PET/MR and PET/CT in the lung for oncological applications, to date, in spite of the increasing research interest for applying PET-based imaging in TB, there have been no studies comparing the two technologies for use in this disease. In general, 18F-FDG PET/MR has been found to perform equally as well as PET/CT in cancer imaging throughout the body [8] but for imaging lung nodules that are small or of low FDG avidity, PET/MRI has been shown to be less good than PET/CT [9-11].

The aim of this study was to assess whether PET/MR is as effective as PET/CT in measuring the extent and activity of PTB lung lesions such that it may be used as an alternative to PET/CT in the burgeoning field of TB functional imaging to monitor the response to therapy in clinical trials.

METHODS AND MATERIALS

Patient cohort

Patients with a clinical diagnosis of PTB were recruited who exhibited characteristic symptoms and compatible X-ray findings plus microbiological confirmation with one or more of (i) sputum AFB smear-positive, (ii) GeneXpert (Cepheid, California, USA) positive or (iii) tuberculosis culture positive. Exclusion criteria were having received tuberculosis treatment for more than 8 weeks, presence of metallic implants that would render MRI unsafe, and the presence of poorly controlled diabetes mellitus. Ten subjects were prospectively recruited. This study was approved by the National Health Group Domain Specific Review Board, Singapore, and informed, written consent was obtained from all participants.

All procedures were performed during a single study visit. Patients received an intravenous injection of 18F-FDG with a mean injected activity of 129.0 ± 4.1 MBq (mean ± s.d.). Five of the ten patients underwent a PET/MR scan (Siemens Biograph mMR, Siemens Healthineers, Erlangen, Germany), followed by PET/CT (Siemens mCT), while the remaining five were imaged first on PET/CT, followed by the PET/MR imaging.

PET/MR acquisition

The PET/MR studies were performed using two 12-channel surface coils. PET data were acquired over the lungs for 15 minutes at 66.7 ± 14.4 minutes (mean ± s.d.) p.i. when performing PET/MR imaging first, and 92.4 ± 7.6 minutes when PET/MR data were acquired second. The PET acquisition was longer than what would typically be acquired clinically (when performing a PET/CT study) as the additional time on the bed is necessary for MR image acquisition. The PET data were reconstructed using OP-OSEM with 3 iterations and 21 subsets. A Gaussian post-smoothing filter of 6 mm full-width at half maximum was applied. The matrix size was 172 × 172, with a voxel size of 4.17 × 4.17 mm and slice thickness of 2.03 mm.

The MR protocol included Dixon imaging for MR-based Attenuation Correction (MRAC), pre- and post-contrast T1-weighted Volumetric Interpolated Breath-hold Examination (VIBE). T2-weighted Half Fourier Acquisition Single Shot Turbo Spin Echo (HASTE) and a navigated three-dimensional

sampling perfection with application optimized contrasts using different flip-angle evolutions (3D-SPACE) sequences were also acquired. MR contrast agent (Magnevist, Bayer HealthCare, Germany) was administered during the scan at a dose of 0.1 mmol/kg. Contrast was not administered to one patient due to a glomerular filtration rate of less than 60 mL/min/1.73m^2. Details of the MR acquisition parameters are given in Table 1.

PET/CT acquisition

Patients underwent a thoracic CT (120 kVp; quality reference mAs = 120; pitch = 1.5; 0.59 × 0.59 × 1.5 mm^3 voxel size) covering the whole lung in either one or two bed positions. With only two bed positions, PET data were acquired for 10 minutes per bed. This was in order to produce data exhibiting a comparable noise level to the PET/MR. The PET/CT study was performed at 61.1 ± 3.9 minutes p.i. when performed first and 117.2 ± 5.6 minutes as the second acquisition. Images were reconstructed with OP-OSEM (3 iterations and 24 subsets) and a 6 mm post-smooth filter. The reconstructed PET image matrix was 200 × 200 with a voxel size of 4.07 × 4.07 mm and slice thickness of 2.03 mm. Time-of-flight and point-spread function modelling capabilities of the PET/CT were not applied to produce images that were comparable with those of the PET/MR.

Image analysis

Visual assessment. Images were analysed by two experienced medical image analysts (8 and 6 years' experience) using a methodology similar to that of Drzezga et al. [12]. The scans were distributed between the two readers such that each assessed 5 PET/CT and 5 PET/MR studies, while not having to rate both scans for an individual patient. The aim was to reduce the possibility of introducing a bias in the detection of a lesion due to prior knowledge acquired from observing the other imaging modality.

For the assessment of the PET/MR studies, the PET data were used to locate regions in the lung parenchyma exhibiting increased uptake. The T2-weighted HASTE and post-contrast T1-weighted VIBE were evaluated for the purposes of anatomical correlation with PET uptake. The PET/CT studies were assessed based on increased PET uptake and the CT image was used to correlate structure with PET uptake. The correlation of structural imaging and PET uptake was rated on a lesion-by-lesion basis using a scale of 0 to 3 (0, no anatomical correlation detectable; 1, uncertain anatomical correlation; 2,

good anatomical correlation; 3, excellent anatomical correlation). The readers were requested to identify all pulmonary lesions in each study. Observations of lymphadenopathy or extra-pulmonary tuberculosis were not included in the analysis. Given these lesions, a subset of 5 lesions per patient were selected based on the order of appearance when viewing axial images from the apex of the lung to the diaphragm. A maximum of 5 lesions per patient were included to avoid an individual patient being over-represented. These subsets were then used for the subsequent quantitative analysis. To ensure that the same lesions were evaluated in both PET images, the readers were required to agree on the subset used for each patient, where all 5 lesions could be identified in both modalities. To compare the background activity in healthy lung between the two scanners, a spherical (diameter: 3.0 cm) volume of interest (VOI) containing normal lung tissue was also determined for each patient.

In addition to the assessment of pulmonary lesions, all studies were graded in terms of: 1) lesion detectability, 2) image quality and 3) global alignment of the PET and structural data. These were scored on a scale of 0 to 3, with 0 representing poor and 3 equating to excellent [12-13].

Quantitative comparison. Quantitative assessment of the PET/MR and PET/CT images was performed through SUV analysis. PET uptake was evaluated by defining a 3D iso-contour on the PET data, containing voxels that were ≥ 50% of the maximum SUV found from a spherical VOI placed over the lesion. SUVmean and SUVmax were measured for the lesion iso-contours and background VOIs. The volumes of the lesion iso-contours were also measured.

A further analysis of the MR mu-maps was undertaken. Each lesion was classified into one of four categories based on the linear attenuation coefficient (LAC) assigned in the MRAC-based mu-map. Lesions were categorised as either soft tissue where the voxels of the segmented lesion were predominantly μ=0.1 cm^{-1}, fat when μ=0.0854 cm^{-1}, lung tissue when μ=0.0224 cm^{-1} or *mixed* where at least 20% of voxels belonged to one tissue class, while the remaining voxels belonged to another. For each lesion VOI (5 per patient) defined on the PET of the PET/CT study, the mean HU was calculated using the CT data. The HU values for the groups were compared.

Statistical analysis

All statistical analysis was undertaken in R (v. 3.2.2) [14]. The visual ratings between PET/CT and PET/MR were assessed using Wilcoxon signed-rank tests for paired samples. For the SUV analysis, an analysis of variance of mixed factorial design with repeated measures was applied to determine the effects of scanner and the time from injection to imaging. Bland-Altman analysis was undertaken to compare PET/CT and PET/MR for the mean and maximum lesion SUVs. A p-value of less than 0.05 was considered significant.

RESULTS

Ten participants with confirmed tuberculosis (age: 54.9 ± 9.7 years [mean ± s.d.]; range: 42.1 - 74.6 years; 7 males) were recruited. Example PET/CT and PET/MR images of a tuberculosis patient are shown in Figure 1. Cavitary, FDG-avid lesions can be observed in the apex of the left lung on both modalities. Figure 2 demonstrates that structural abnormalities, as seen on CT (Figure 2A), can be identified using the post-contrast T1w-VIBE (Figure 2C). The T2w-HASTE exhibits increased signal intensity when fluid is present. A large pleural effusion can be observed with both MR (Figure 2G) and CT (Figure 2E).

A total of 108 PTB lesions were detected on PET/MR and 112 on PET/CT. The four lesions that were not observed on PET/MR all had low mean SUVs (≤ 1.3). Two missed lesions were in the middle lobe and two in the lower lobe, where the effects of respiratory motion are greater. The visual ratings of overall lesion detectability, image quality and alignment are shown in Table 2. There was no significant difference between PET/CT and PET/MR on the three measures. The rating of anatomical correlation between PET lesions and the associated structural imaging is given in Table 3. The highest agreement was found between PET and CT (2.8 ± 0.7), with similar agreement for the T1w-VIBE (2.5 ± 0.7) and T2w-HASTE (2.4 ± 0.6).

Measured mean and maximum lesion SUVs were significantly lower on PET/MR compared to PET/CT. The mean (± s.d.) SUVmean was 2.6 ± 1.4 on PET/MR and 3.5 ± 1.5 on PET/CT ($p = 0.0005$). Mean SUVmax was 4.3 ± 2.5 on PET/MR and 5.3 ± 2.4 on PET/CT ($p = 0.02$). Bland-Altman analysis (Figure 3) confirmed the lower SUVmean and SUVmax values with PET/MR, but demonstrated substantial variability. A significant effect of the time between injection and the commencement of imaging was found for SUVmean ($p = 0.039$) and SUVmax ($p = 0.049$). The mean time from injection to PET/CT imaging was 89.1 ± 29.9 minutes and 79.5 ± 17.4 minutes for PET/MR.

It should also be noted that differences were observed in SUVmean and SUVmax when calculated according to the scan order. When performing PET/CT first, the mean SUVmean was 3.9 ± 1.3 for PET/CT and 3.3 ± 1.5 for PET/MR (SUVmax: PET/CT: 5.7 ± 2.0; PET/MR: 5.5 ± 2.2). In the subjects

where PET/MR imaging was performed first, the average SUVmean was 3.2 ± 1.6 for PET/CT and 1.7 ± 1.0 on PET/MR (SUVmax: PET/CT: 4.0 ± 2.7; PET/MR: 3.0 ± 2.1).

In terms of the background VOIs, the average SUVmean was 0.4 ± 0.1 on PET/MR and 0.5 ± 0.1 on PET/CT (p=0.26) and the average SUVmax was 0.7 ± 0.2 on PET/MR and 0.7 ± 0.2 on PET/CT (p=0.60). No significant difference was observed in the lung background, suggesting that the SUVs observed in healthy lung tissue are comparable between the two scanners.

The median (range) observed lesion volume was 4.9 (0.5 – 101.0) cm^3 when imaging with PET/CT and 5.1 (0.8 – 114.7) cm^3 for PET/MR (p=0.17). While the smallest lesion volume observed with PET/CT was 0.5 cm^3, whereas with PET/MR the smallest volume seen was 0.8 cm^3, the volumes delineated by the readers were not significantly different between the imaging two modalities.

All lesions were classified based on the LACs assigned to each lesion in the mu-map. Of the 50 lesions, 19 were identified as soft tissue, 23 as lung, 0 as fat and 8 as a mixture of lung and soft tissue. The mean (± s.d) of the HU values was -258 ± 172 in lung group, -242 ± 126 for mixed lesions and -171 ± 160 soft tissue. The HU values for each group are shown in figure 4. The majority of lesions (36/50) had a mean HU of between -300 and 30. This demonstrates that most PTB lesions had an average density between lung tissue and fluid.

Figure 5 shows an example from a subject where a large, cavitary PTB lesion has been misclassified as lung tissue in the MRAC mu-map. The SUVmax of the lesion was 38% lower with PET/MR compared to PET/CT (SUVmean: -36%).

No calcified lesions or miliary PTB were observed. Increased MR signal intensity was observed in the lymph nodes of two patients which may represent inflammation or caseosis [15]. Osseous TB was not observed in any patients with either imaging modality. However, this is not surprising as participants were selected on the basis of having PTB. Bone involvement is rare in this condition. In addition, due scanning time constraints, specific MR imaging of the spine, for example, was not performed.

DISCUSSION

In general, this study has shown that PET/MR is qualitatively comparable to PET/CT, with all but four lesions seen on PET/CT also being visualised on PET/MR. The lesions that were not detected with PET/MR had low SUVs as measured on PET/CT. In addition, these were small (<1cm along the longest axis) and may be at the limits of what is detectable with MR. The location of the missed lesions in the middle and lower lobes, suggest that respiratory motion may have played a role in the misdetection of these lesions. There were no patients in whom this would have meant a diagnosis of active tuberculosis being missed because there were FDG-avid lesions, indicative of PTB, visible on PET/MR, in all cases.

Measures of overall image quality and anatomical alignment were also similar between PET/MR and PET/CT. This is despite the additional challenges posed by effects of respiratory motion and susceptibility artefacts in acquiring good quality MR images of the lungs. In our protocol, we attempted to control for this by acquiring MR data using both breath-held (HASTE and VIBE) or navigated sequences (SPACE). Nevertheless, artefacts due to respiratory motion were present as some tuberculosis patients had difficulty complying with breath-holding instructions.

Significantly lower SUVs were observed on PET/MR compared to PET/CT, both for SUVmean and SUVmax. Although we sought to mitigate the impact of changes in uptake over time, by varying the order of scans (half had PET/MR first and half had PET/CT first), and by minimising the time between the two scans (maximum: 62 minutes), the time between injection and imaging was found to have a significant effect. This suggests that 18F-FDG accumulation continues to change beyond 60 minutes in PTB lesions. Dual time-point imaging with 18F-FDG PET/CT has previously shown a median increase of 13% in the SUVmax of tuberculomas when comparing images at 60 and 120 minutes [16]. Thus, although the time between 18F-FDG dose and PET/MR was longer than with PET/CT, this time difference would likely explain only a small proportion of the observed difference in SUV between the two scanners and this is likely due mainly to attenuation correction errors caused by the linear attenuation coefficients assigned in the lung [17].

In this study, most PTB lesions were identified by MRAC as either lung tissue or a mixture of lung and soft tissue. When compared to the measured CT data, it is clear that applying these LACs will result in an underestimation of attenuation and will therefore result in an underestimation of the activity in the area of the lesion. Attenuation correction factors can be calculated from CT transmission data. It is not possible to directly measure radiodensity with MRI. Dixon-based MRAC is known to affect the quantitative accuracy of PET/MR data. The differences in SUVs between the two modalities observed in this study are larger than those seen when imaging other parts of the body [17-18]. Mapping MR image intensities to appropriate attenuation coefficients has been shown to be problematic [19]. The current Dixon-based MRAC method assigns uniform attenuation coefficients in the lung.

The use of uniform coefficients results in both over-estimation of regions that are closer to air and dramatically under-estimates the true attenuation coefficients of tuberculosis lesions. This effect is demonstrated in Figure 5 where a large, cavitary lesion is clearly visible on the mu-map derived from CT, but is entirely absent from the MRAC-based mu-map. The lesion has been assigned a lung attenuation coefficient in the MR mu-map. The SUVmax of the lesion was dramatically lower with PET/MR compared to PET/CT. It is unclear how to accurately determine attenuation coefficients in, for example, areas of caseous necrosis commonly seen in tuberculosis. This study has shown that there is large variability in the density of PTB lesions, further suggesting that a uniform attenuation coefficient is insufficient to accurately represent the types of lesions seen in tuberculosis.

While this study has shown that overall the SUVs may be lower when imaging with PET/MR, this reduction would be consistent between longitudinal scans, so increases or decreases of SUV within a single patient can be used to monitor treatment response using PET/MR in research applications in PTB.

CONCLUSION

This study has shown that visual detection of PTB lesions is comparable between PET/MR and PET/CT. Although the values of SUVmax and SUVmean are significantly lower with PET/MR, research applications measuring the response of lung lesions in response to therapy, are unlikely to be affected by these differences in quantification. PET/MR offers the advantage of reduced radiation exposure to participants with an essentially curable disease.

ACKNOWLEDGEMENTS

The authors would like to thank Yap Tian Siew and Ng Stevia Lay Hong at CIRC.

Compliance with Ethical Standards

Funding: This research is part of the Singapore Programme of Research Investigating New Approaches to Treatment of Tuberculosis and was supported by the Singapore Ministry of Health National Medical Research Council under its TCR Flagship Grant NMRC/TCR/011-NUHS/2014, its CS-IRG Grant NMRC/CIRG/1322/2012, and its Center Grant NMRC/CG/013/2013, and by National University of Singapore under its Start-up Grant.

Conflict of interest: All authors declare that they have no conflicts of interest.

Ethical approval: All procedures performed in studies involving human participants were in accordance with the ethical standards of the institutional and/or national research committee and with the 1964 Helsinki declaration and its later amendments or comparable ethical standards.

Informed consent: Informed consent was obtained from all individual participants included in the study.

REFERENCES

1. Chen RY, Dodd LE, Lee M, et al. PET/CT imaging correlates with treatment outcome in patients with multidrug-resistant tuberculosis. 2014;265.

2. Esmail H, Lai RP, Lesosky M et al. Characterization of progressive HIV-associated tuberculosis using 2-deoxy-2-[18F]fluoro-d-glucose positron emission and computed tomography. Nat Med. 2016;22:1090–1093.

3. Malherbe ST, Shenai S, Ronacher K et al. Persisting positron emission tomography lesion activity and Mycobacterium tuberculosis mRNA after tuberculosis cure. Nat Med. 2016;22:1094–1100.

4. Glaudemans AWJM, Signore A. FDG-PET/CT in infections: The imaging method of choice? Eur J Nucl Med Mol Imaging. 2010;37:1986-1991.

5. Skoura E, Zumla A, Bomanji J. Imaging in tuberculosis. Int J Infect Dis. 2015;32:87-93.

6. Vorster M, Sathekge MM, Bomanji J. Advances in imaging of tuberculosis: the role of 18F-FDG PET and PET/CT. Curr Opin Pulm Med. 2014;20:287-293.

7. Soussan M, Brillet PY, Mekinian A, et al. Patterns of pulmonary tuberculosis on FDG-PET/CT. Eur J Radiol. 2012;81:2872-2876.

8. Spick C, Herrmann K, Czernin J. 18F-FDG PET/CT and PET/MRI perform equally well in cancer patients: Evidence from studies in more than 2300 patients. J Nucl Med. 2016;57:1-38.

9. Stolzmann P, Veit-Haibach P, Chuck N, et al. Detection Rate, Location, and Size of Pulmonary Nodules in Trimodality PET/CT-MR Comparison of Low-Dose CT and Dixon-Based MR Imaging. Invest Radiol. 2013;48:241-246.

10. Sawicki LM, Grueneisen J, Buchbender C, et al. Evaluation of the Outcome of Lung Nodules Missed on 18F-FDG PET/MRI Compared with 18F-FDG PET/CT in Patients with Known Malignancies. J Nucl Med. 2016;57:15-20.

11. Sawicki LM, Grueneisen J, Buchbender C, et al. Comparative Performance of 18F-FDG PET/MRI and 18F-FDG PET/CT in Detection and Characterization of Pulmonary Lesions in 121 Oncologic Patients. J Nucl Med. 2016;57:582-586.

12. Drzezga A, Souvatzoglou M, Eiber M, et al. First Clinical Experience with Integrated Whole-Body PET/MR: Comparison to PET/CT in Patients with Oncologic Diagnoses. J Nucl Med. 2012;53:845-855.

13. Eiber M, Martinez-Möller A, Souvatzoglou M, et al. Value of a Dixon-based MR/PET attenuation correction sequence for the localization and evaluation of PET-positive lesions. Eur J Nucl Med Mol Imaging. 2011;38:1691-1701.

14. R Core Team. R: A Language and Environment for Statistical Computing. 2013. http://www.r-project.org/.

15. Rizzi EB, Schinina' V, Cristofaro M, et al. Detection of Pulmonary tuberculosis: comparing MR imaging with HRCT. BMC Infect Dis. 2011;11:243.

16. Sathekge MM, Maes A, Pottel H, et al. Dual time-point FDG PET / CT for differentiating benign from malignant solitary pulmonary nodules in a TB endemic area. S Afr Med J. 2010;100:598-601.

17. Vandenberghe S, Marsden PK. PET-MRI: a review of challenges and solutions in the development of integrated multimodality imaging. Phys Med Biol. 2015;60:R115-54.

18. Samarin A, Burger C, Wollenweber SD, et al. PET/MR imaging of bone lesions - Implications for PET quantification from imperfect attenuation correction. Eur J Nucl Med Mol Imaging. 2012;39:1154-1160.

19. Wagenknecht G, Kaiser H-J, Mottaghy FM, et al. MRI for attenuation correction in PET: methods and challenges. Magn Reson Mater Physics, Biol Med. 2013;26:99-113.

Figures

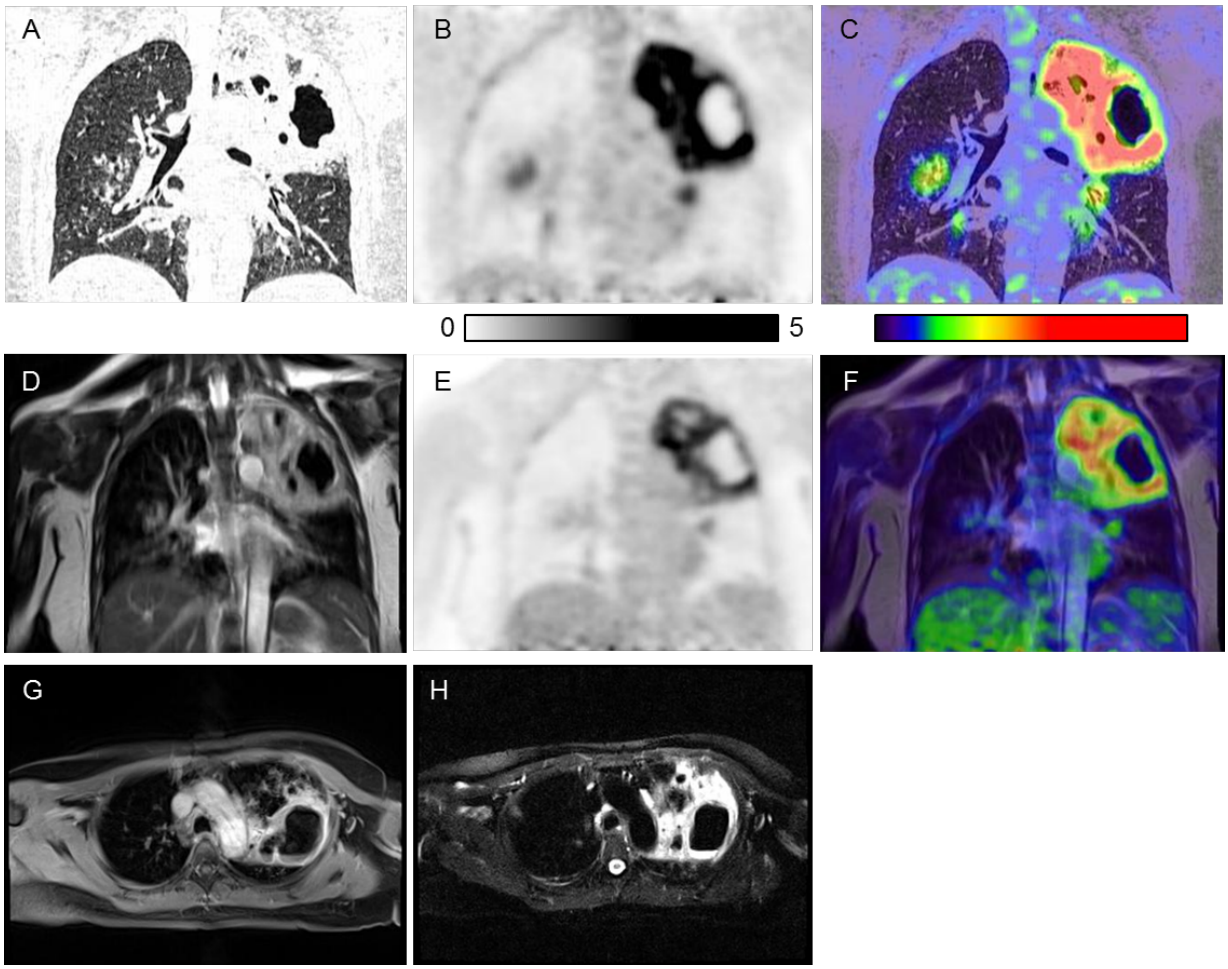

Figure 1. Example images of a tuberculosis patient. Top row: coronal PET/CT images of CT (A), PET (B) and fused PET/CT (C). Middle row: coronal PET/MR images of T2-weighted 3D-SPACE (D), PET (E) and fused data (F). Bottom row: axial T1-weighted VIBE (G) and T2-weighted HASTE (H).

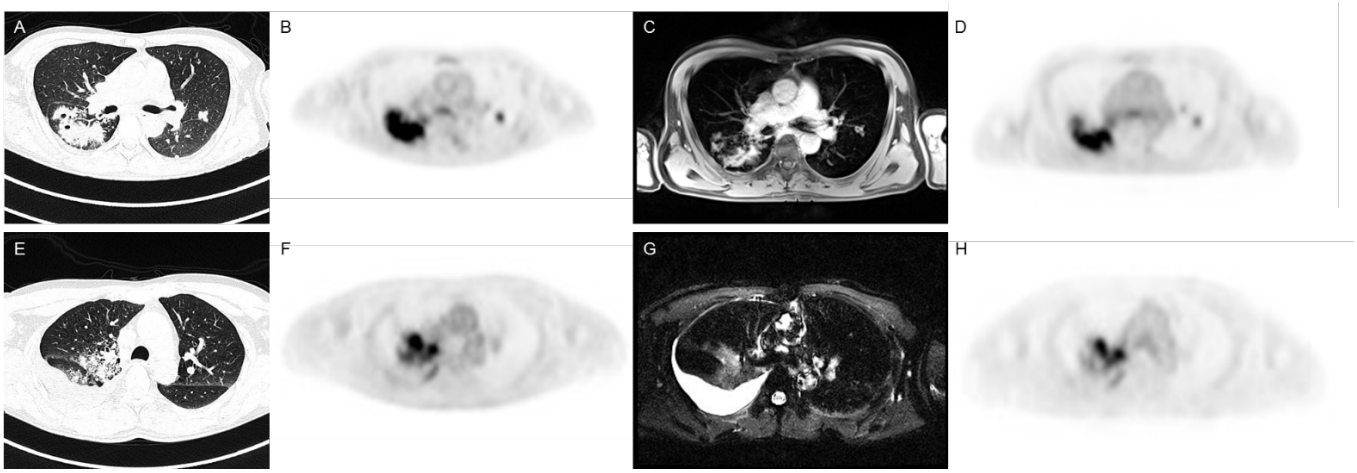

Figure 2. PET/CT and PET/MR images of two patients. Top row: axial images of CT (A) and the associated PET (B), and T1-weighted VIBE (C) with the PET data (D). Bottom row: axial CT (E) and PET (F), and T2-weighted HASTE (G) with the associated PET (H).

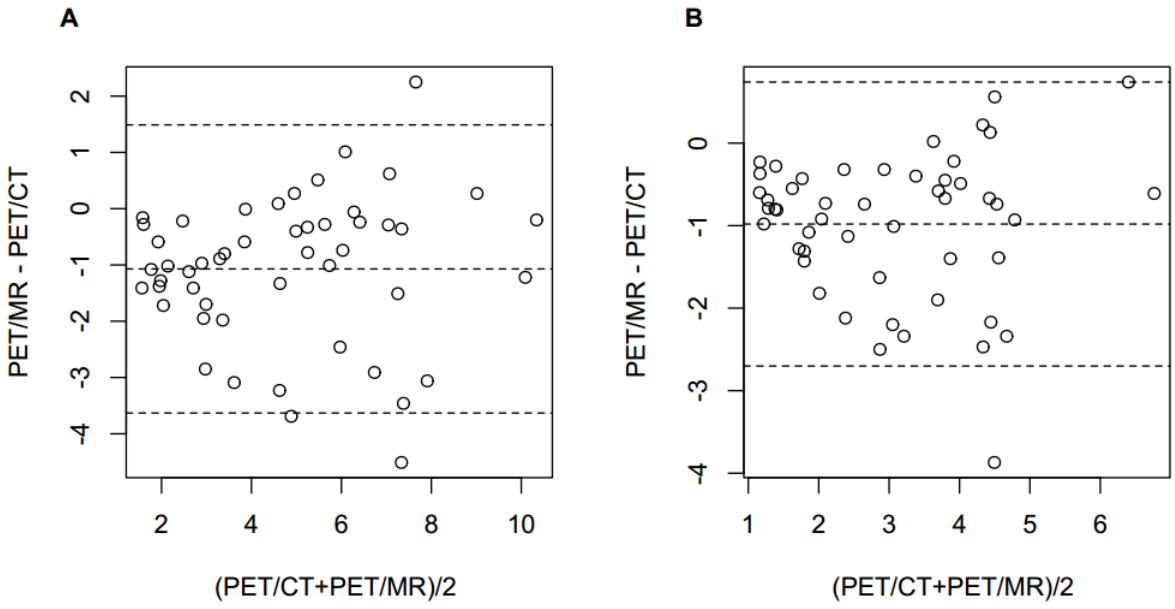

Figure 3. Bland-Altman plots of SUVmax (A) and SUVmean (B). The dashed lines represent the mean ± 1.96 s.d. .

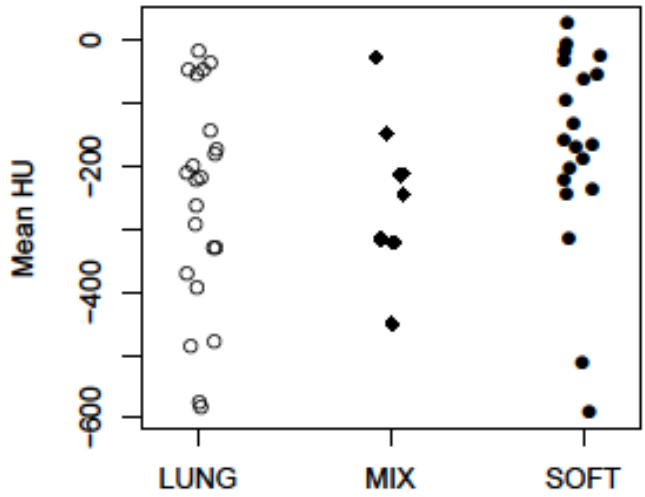

Figure 4. The mean HU for each lesion measured on the PET/CT study, separated into groups based on MR mu-map tissue classification. The lung tissue (LUNG), soft tissue (SOFT) and mixed (MIX) lesion groups are shown; no lesions were identified as fat.

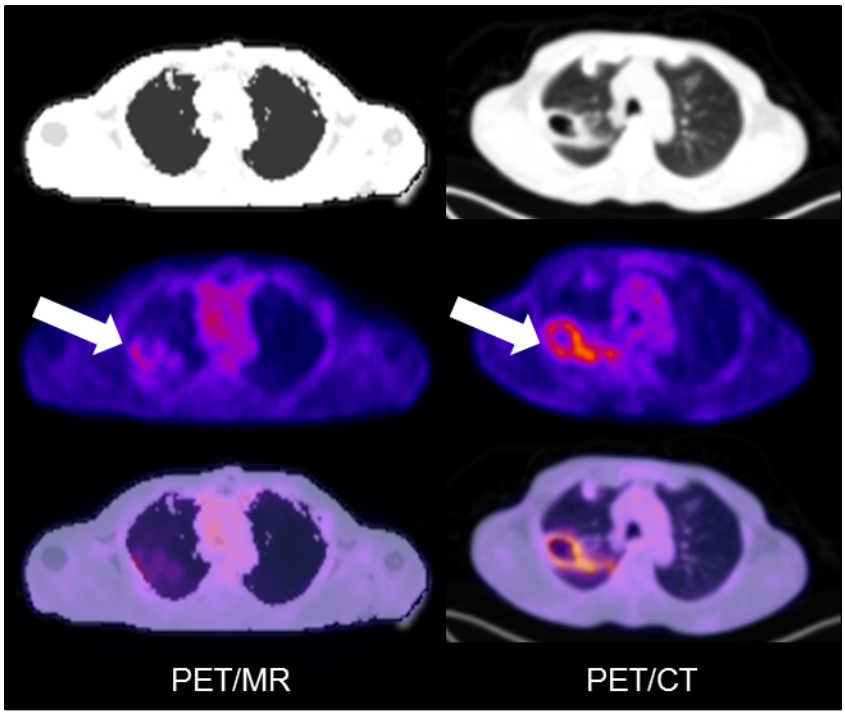

Figure 5. Large, cavitary lung lesion in right lung of a tuberculosis patient imaged on PET/MR (left column) and PET/CT (right column). Mu-maps for attenuation correction (top), SUV images (middle) and fused images (bottom). Lesion (arrows) SUVmax was 2.1 on PET/MR and 3.4 on PET/CT. SUVmean was 1.4 ± 0.3 (PET/MR) and 2.2 ± 0.4 (PET/CT).

Tables

Sequence	TR (ms)	TI (ms)	TE (ms)	Resolution (mm)	Orientation	FA (^{0})	BW (Hz)	FoV (mm)
Dixon	3.6	-	1.23	2.60×2.60×3.12	Coronal	10^0	965	500×328
T2w-HASTE	1960	240	95	1.09×1.09×5.00	Axial	160^0	710	350×263
T2w-SPACE	5103	-	100	1.09×1.09×5.00	Coronal	170^0	657	350×350
T1w-VIBE*	4.07	-	1.79	1.09×1.09×5.00	Axial	5^0	539	350×263

Table 1. Acquisition parameters of the MRI sequences: repetition time (TR), inversion time (TI), echo time (TE), flip angle (FA), bandwidth (BW) and field-of-view (FoV). *T1w-VIBE was performed twice, once before and five to ten minutes after administration of MR contrast.

	PET/CT	PET/MR	p-value
Lesion detectability	2.9 ± 0.3	2.7 ± 0.5	0.42
Image quality	2.9 ± 0.3	2.6 ± 0.5	0.23
Alignment	2.6 ± 0.7	2.4 ± 0.5	0.57
Total no. lesions	112	108	-
Lesion volume (cm^3) [median (range)]	4.9 (0.5 – 101.0)	5.1 (0.8 – 114.7)	0.17

Table 2. Analysis of PET/CT and PET/MR.

	Anatomic correlation rating [mean ± s.d.]
CT	2.8 ± 0.7
T1w-VIBE	2.5 ± 0.7
T2w-HASTE	2.4 ± 0.6*

Table 3. Rating of the anatomical correlation (0-3) between the PET and structural imaging. *Significantly lower rating than CT (p = 0.023).